*Anal. Chem.* **1999,** *71,* 3928−3934

# Near-Infrared Surface Plasmon Resonance Measurements of Ultrathin Films. 1. Angle Shift and SPR Imaging Experiments

Bryce P. Nelson, Anthony G. Frutos, Jennifer M. Brockman, and Robert M. Corn*

*Department of Chemistry, University of Wisconsin—Madison, 1101 University Avenue, Madison, Wisconsin 53706-1396*

**The application of surface plasmon resonance (SPR) measurements to the study of ultrathin organic and inorganic films adsorbed onto gold surfaces utilizing near-infrared (NIR) excitation from 800 to 1152 nm is described. SPR scanning angle measurements of film thickness are demonstrated at 814 and 1152 nm using low-power diode and HeNe laser sources, respectively. Several advantages of SPR in the NIR are noted. The in situ reflectivity versus angle of incidence curves sharpen greatly (as compared to 632.8 nm) at longer wavelengths so that there is no loss in sensitivity in the measurement of film thickness despite a doubling of the excitation wavelength. The sharper resonance and longer wavelengths also allow for the measurement of thicker films. Examples of SPR thickness measurements for self-assembled alkanethiol monolayers and composite biopolymer/$SiO_2$ nanoparticle electrostatic multilayer films are given. SPR imaging experiments are also performed at various NIR wavelengths using an incoherent white light source and narrow band-pass filters. The incoherent white light source eliminates laser fringes that have been observed in previous SPR imaging experiments, and the use of narrow band-pass filters allows for the easy selection and variation of excitation wavelength. The narrowness of the reflectivity versus angle curves leads to greater contrast in NIR SPR images compared to the same features examined with excitation from visible light. The combination of these changes results in nearly 1 order of magnitude enhancement in the SPR differential reflectivity image, indicating that SPR imaging is best conducted with incoherent NIR excitation. One disadvantage of using NIR wavelengths for SPR imaging is that the surface plasmon propagation length increases in the NIR so that the lateral image resolution is reduced; however, image features larger than 50 $\mu$m can easily be resolved. A NIR SPR image of a DNA array onto which single-stranded DNA binding protein has bound is shown as an example of how NIR SPR imaging experiments have sufficient sensitivity to monitor DNA−protein interactions.**

Surface plasmon resonance (SPR) measurements are surface-sensitive optical methods for the characterization of ultrathin films adsorbed onto gold or other noble metal surfaces.[1,2] For example, the very successful Biacore instrument measures protein/protein interactions by using SPR reflectivity measurements to follow the uptake of molecules from aqueous solution into a chemically modified dextran layer attached to a gold thin film.[3−5] The adsorption of self-assembled alkanethiol monolayers onto gold surfaces both in air (ex situ) and in water (in situ) has been extensively characterized with SPR techniques.[2,6−10] The ability of SPR techniques to monitor thin-film growth in situ permits the characterization of ultrathin monolayers and multilayers under a variety of conditions (e.g., monitoring biopolymer adsorption from complex buffer solutions, following structural changes during electrochemical or thermal cycling).[9,11,12] In addition, adsorption and film growth onto patterned surfaces can be followed with SPR imaging experiments (e.g., the assay of antibodies with antigen arrays, the sequence-specific binding of proteins onto DNA arrays).[6,10]

A typical SPR "scanning angle" experiment monitors the reflectivity of an incident light beam from a gold thin film attached to a glass prism as a function incident angle. For example, Figure 1 plots the reflectivity versus angle of incidence for a 632.8-nm HeNe laser from a prism/gold film/water assembly. At a specific angle in the SPR reflectivity curve, a pronounced minimum occurs. At this angle, defined as the "SPR angle", surface plasmon polaritons (SPPs) are created at the gold/water interface. SPPs propagate parallel to the gold surface, and the intensity of the optical electric fields associated with a SPP decays exponentially away from the surface with a decay length on the order of 200 nm. The momentum of a SPP is sensitive to the index of refraction inside this decay length. Changes in the local index of refraction upon adsorption of organic monolayers or multilayers result in

(1) Homola, J.; Yee, S. S.; Gauglitz, G. *Sens. Actuators B* **1999**, *54*, 3−15.
(2) Frutos, A. G.; Corn, R. M. *Anal. Chem.* **1998**, *70*, 449A−455A.
(3) Fägerstam, L. G.; O'Shannessy, D. J. In *Handbook of Affinity Technology*; Kline, T., Ed.; Marcel Dekker: New York, 1993; Vol. 63, pp 229−252.
(4) Malmqvist, M. *Biochem. Soc. Trans.* **1999**, *27*, 335−340.
(5) Löfås, S.; Malmqvist, M.; Rönnberg, I.; Stenberg, E.; Liedberg, B.; Lundström, I. *Sens. Actuators B* **1991**, *5*, 79−84.
(6) Frey, B. L.; Jordan, C. E.; Kornguth, S.; Corn, R. M. *Anal. Chem.* **1995**, *67*, 4452−4457.
(7) Hanken, D. G.; Corn, R. M. *Anal. Chem.* **1995**, *67*, 3767−3774.
(8) Peterlinz, K. A.; Georgiadis, R. *Opt. Commun.* **1996**, *130*, 260−266.
(9) Jordan, C. E.; Frey, B. L.; Kornguth, S.; Corn, R. M. *Langmuir* **1994**, *10*, 3642−3648.
(10) Jordan, C. E.; Corn, R. M. *Anal. Chem.* **1997**, *69*, 1449−1456.
(11) Brockman, J. M.; Frutos, A. G.; Corn, R. M. *J. Am. Chem. Soc.*, in press.
(12) Hanken, D. G.; Corn, R. M. *Anal. Chem.* **1997**, *69*, 3665−3673.



10.1021/ac990517x CCC: $18.00 
Published on Web 08/18/1999

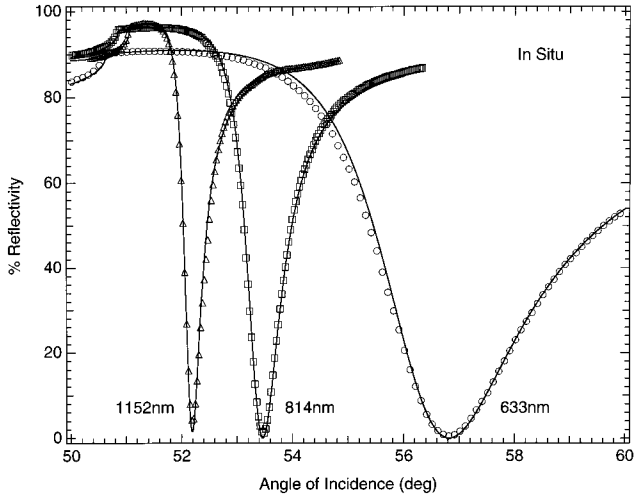


Figure 1. SPR reflectivity curves of p-polarized light as a function of incident angle, $\theta$, for an SF-10 glass/Au/water (in situ) assembly with (△) 1152-, (□) 814-, and (○) 633-nm excitation. Solid lines show the results of a three-phase complex Fresnel calculation. For each wavelength, the thickness of the gold was optimized to minimize reflectivity at the SPR minimum. Gold thicknesses of 47.5, 45.0, and 40.0 nm were used for the 633-, 814-, and 1152-nm excitation, respectively. Reflectivity curves sharpen with increasing wavelength, the result of more favorable optical properties of gold in the near-infrared compared to that in the visible region. The increased sharpness facilitates certain angle scan measurements and improves contrast in SPR imaging.

changes in the SPR angle. This SPR "angle shift" measurement is used to follow adsorption onto a chemically modified gold surface. In contrast, the SPR imaging experiment monitors changes in the reflectivity image at a fixed angle from a patterned surface in order to monitor the simultaneous adsorption of analyte onto arrays of chemical functionalities.

Although most SPR scanning angle shift measurements on gold surfaces use a 632.8-nm HeNe laser as the excitation source, SPR measurements on gold can in principle be obtained at any wavelength longer than the interband transition at 520 nm.[13] For example, SPR angle shift measurements have been made previously in the near-infrared (NIR) out to 3.39 $\mu$m.[1,14−23] For cases where the adsorbing molecules have a strong absorption band in the visible region, the analysis of SPR angle shift measurements can be simplified by using NIR excitation. Different wavelengths can also be employed in the SPR imaging experiment; one previous study employed broad-band visible illumination for the SPR imaging of copper phthalocyanine thin films.[24]

In this paper, we demonstrate the benefits of using NIR light for SPR angle shift and SPR imaging measurements. As can be seen in Figure 1, use of NIR excitation in SPR scanning angle experiments changes the position and sharpness of the SPR angle. We show that for SPR angle shift measurements, despite a substantial increase in excitation wavelength in the NIR, the adsorption of thin films and monolayers down to 0.2 nm can still be observed. In addition, the dynamic range of the SPR angle shift measurements is expanded in the NIR, and the formation of multilayer films up to 35 nm can now be easily monitored. The sharpening of the SPR reflectivity minimum in the NIR also leads to improvements in the SPR imaging experiment; an increase in the differential reflectivity near the SPR angle results in an enhancement of the contrast in the NIR SPR images. In addition, we show that an incoherent white light source and a narrow band-pass filter can be used to obtain SPR images at NIR wavelengths and eliminates the laser fringes that are observed in the SPR images obtained with coherent sources. To demonstrate enhancement of image quality in the narrow band-pass NIR SPR imaging experiments, the adsorption of single-stranded DNA binding protein (SSB) onto an array of single-stranded DNA molecules is monitored.

## EXPERIMENTAL CONSIDERATIONS

**Materials.** 11-Mercaptoundecanoic acid (MUA; Aldrich), 11-mercaptoundecanol (MUD, synthesized as described previously),[25] 11-mercaptoundecylamine (MUAM, synthesized by the Whitesides group and described elsewhere),[26] poly(L-lysine) hydrobromide (PL) (MW 34 300; Sigma), and poly(L-glutamate) (PG) (MW 95 000; Sigma) were used as received. Reagents and details for the DNA/single-stranded binding protein adsorption measurement are found elsewhere.[11,27,28] Absolute ethanol (Aaper) and Millipore-filtered water were used for rinsing and for aqueous solutions. Colloidal suspensions were prepared via the sol−gel method. Base-hydrolyzed $SiO_2$ suspensions were synthesized from tetraethyl orthosilicate (Aldrich) as described elsewhere.[29] The final pH and concentration of the $SiO_2$ sol were 8.8 and 25 mg/mL, respectively. The suspension was filtered through 0.45-$\mu$m HA filters (Millipore) and was stable for several months.

**Thin-Film Preparation Methods.** SPR experiments utilized thin (37.5−45 nm) gold films vapor deposited onto BK-7 or SF-10 glass slides (18 × 18 mm) as described previously.[9] In the case of the SPR imaging experiments, a thin (<1 nm) chromium underlayer was used to enhance the adhesion of gold to the SF-10 slide. For MUA and MUD monolayer formation, gold-coated slides were immersed in a 1 mM ethanolic solution for at least 2 h and subsequently rinsed with ethanol and water. Alternating PL and PG multilayers were formed by immersing a MUA-coated sample sequentially in aqueous solutions of PL and PG for 30 min

(13) Aust, E. F.; Sawodny, M.; Ito, S.; Knoll, W. *Scanning* **1994**, *16*, 353−361.
(14) Berger, C. E. H.; Kooyman, R. P. H.; Greve, J. *Rev. Sci. Instrum.* **1994**, *65*, 2829−2836.
(15) de Bruijn, H. E.; Kooyman, R. P. H.; Greve, J. *Appl. Opt.* **1992**, *31*, 440−442.
(16) Bradberry, G. W.; Sambles, J. R. *Opt. Commun.* **1988**, *67*, 404−408.
(17) Brink, G.; Sigl, H.; Sackmann, E. *Sens. Acuators B* **1995**, *24−25*, 756.
(18) Jorgenson, R. C.; Jung, C.; Yee, S. S. *Sens. Actuators B* **1993**, *13−14*, 721−722.
(19) Hanning, A.; Roeraade, J.; Delrow, J. J.; Jorgenson, R. C. *Sens. Actuators B* **1999**, *54*, 25−36.
(20) Johnston, K. S.; Karlsen, S. R.; Jung, C. C.; Yee, S. S. *Mater. Chem. Phys.* **1995**, *42*, 242−246.
(21) Tubb, A. J. C.; Payne, F. P.; Millington, R. B.; Lowe, C. R. *Sens. Actuators B* **1997**, *41*, 71−79.
(22) Jorgenson, R. C.; Jung, C.; Yee, S. S.; Burgess, L. W. *Sens. Actuators B* **1993**, *13−14*, 721−722.
(23) Karlsen, S. R.; Johnston, K. S.; Yee, S. S.; Jung, C. C. *Sens. Actuators B* **1996**, *32*, 137−141.
(24) Knobloch, H.; Szada-Borryszkowski, G. v.; Woigk, S.; Helms, A.; Brehmer, L. *Appl. Phys. Lett.* **1996**, *69*, 2336−2337.
(25) Frey, B. L.; Hanken, D. G.; Corn, R. M. *Langmuir* **1993**, *9*, 1815−1820.
(26) Tien, J.; Terfort, A.; Whitesides, G. M. *Langmuir* **1997**, *13*, 5349−5355.
(27) Frutos, A. G.; Smith, L. M.; Corn, R. M. *J. Am. Chem. Soc.* **1998**, *120*, 10277−10282.
(28) Jordan, C. E.; Frutos, A. G.; Thiel, A. J.; Corn, R. M. *Anal. Chem.* **1997**, *69*, 4939−4947.
(29) Chu, L.; Anderson, M. A. *J. Membr. Sci.* **1996**, *110*, 141.

each. After each step, the sample was rinsed with water for 30 s and dried with nitrogen gas. Both polymer solutions were prepared in 50 mM borate buffer solutions with a concentration of 2 mg/mL. After three polymer layers, negatively charged $SiO_2$ colloids were adsorbed onto the positively charged PL to form a polymer/colloid composite film. Polymer solutions were adjusted to pH 8.8 with NaOH to match the pH of the $SiO_2$ sol. For the in situ adsorption measurements, the concentration of the polymers was 0.1 mg/mL and 5 mM borate buffer was used. Samples were photopatterned by illumination from a mercury−xenon arc lamp (Oriel) for 1 h at 400 W utilizing a mask on a quartz substrate. Samples were rinsed thoroughly with ethanol after photopatterning.

**Scanning SPR Measurements.** The scanning SPR apparatus was composed of a 632.8-nm HeNe laser (4 mW, Uniphase), an 814.5-nm diode laser (1 mW, Melles-Griot), and an 1152-nm HeNe laser (2 mW, Research Electrooptics). The apparatus measures the reflectivity of p-polarized light as a function of the incident angle, $\theta$, in the Kretschmann configuration as described previously.[2,9] A BK-7 hemispherical prism ($n = 1.515$ at 632.8 nm) and gold-coated slides were used for ex situ measurements. Ethylene glycol was used as an index-matching fluid. For in situ measurements, an SF-10 hemispherical prism ($n = 1.727$ at 632.8 nm), gold coated SF-10 slides, and Cargille index matching fluid ($n = 1.730$) were used. Experimental results were fit with an N-phase Fresnel calculation as outlined by Hansen,[30] and available on our website, http://corninfo.chem.wisc.edu. The calculations account for the wavelength dispersion of glass, gold, and water.

**White Light SPR Imaging Apparatus.** The details of a SPR imaging apparatus using 632.8-nm laser excitation have been described previously.[10] In the white light imaging apparatus, light from a 35-W quartz−halogen bulb was focused onto a 0.012-in. pinhole and recollimated by a camera lens. The collimated light passes through a polarizer, strikes the sample at a specified incident angle, and is reflected and detected with an inexpensive CCD camera (iSC2050, i Sight, Inc.) after passing through a narrow-band interference (band-pass) filter. The measured power of the white light source was approximately 0.25 mW before the narrow band filter. Images were examined using NIH Image software on a microcomputer.

## RESULTS AND DISCUSSION

**NIR SPR Reflectivity Curves.** SPPs can be created on the surface of a gold thin film at energies lower than the interband transition at 520 nm.[13] For example, most SPR measurements employ a low power HeNe laser at 632.8 nm. The reflectivity at 632.8 nm measured as a function of incident angle for an SF-10 prism/45.0-nm gold film/water assembly is plotted in Figure 1. The solid line through the points is the fit of a three-phase Fresnel calculation where the complex index of refraction for the 45.0-nm Au film is 0.210 + 3.511i. (The indexes of refraction for the other phases are listed in Table 1.) This SPR reflectivity curve exhibits a broad minimum at 56.82° at which point SPPs are created at the gold/water interface. SPPs propagate parallel to the gold/water interface, and the intensity of the optical electric fields associated with a SPP decays exponentially away from the metal surface with a typical decay length into the aqueous phase on the order of 200 nm. The momentum of a SPP on the surface is sensitive to the index of refraction inside this decay length; changes in the local index of refraction upon adsorption of organic monolayers or multilayers result in a shift in the angle of the SPR reflectivity minimum. The quantitation of the shift of the SPR angle is the basis of most SPR adsorption sensors.

Table 1. Experimentally Determined Optical Constants Used for Fresnel Calculations

| | 632.8 nm | 814 nm | 1152 nm |
|---|---|---|---|
| Au thickness (nm) | 47.5 | 45.0 | 40.0 |
| *n*Au | 0.210 | 0.165 | 0.330 |
| *k*Au | 3.511 | 5.205 | 7.930 |
| *n*SF-10 | 1.723 | 1.711 | 1.700 |
| *n*BK-7 | 1.515 | 1.501 | 1.511 |
| $n H_2O$ | 1.332 | 1.327 | 1.322 |

Also plotted in Figure 1 are the SPR reflectivity curves for 814- and 1152-nm excitation. The gold film thickness is 45.0 and 40.0 nm for the two wavelengths, respectively. The reflectivity minimum associated with the SPR angle sharpens at the longer NIR wavelengths and shifts closer to the critical angle (which also changes slightly due to changes in the prism and water indexes of refraction with wavelength). Fresnel calculation fits are plotted in the figure as solid lines. The optical constants used for these fits are listed in Table 1. As reported in previous work,[31] the imaginary part of the index of refraction for the gold film increases significantly at longer wavelengths, indicative of the fact that the gold film is less lossy at lower optical frequencies. With this increased conductivity, the surface plasmon propagation length on the surface increases in the NIR. We find that the sharpening of the SPR reflectivity minimum in the NIR enables us to measure film thicknesses at 1152 nm with sensitivity equal to or better than that at 632.8 nm, despite the large increase in excitation wavelength.

**Fresnel Reflectivity Calculation Contour Plots.** To describe the variation of the SPR reflectivity curves with wavelength, we employ the 2-D reflectivity contour plots shown in Figures 2 and 3. These contour plots are generated from complex three-phase Fresnel calculations that predict the reflectivity as a function of incident angle and wavelength for the SF-10 prism/gold film/water assembly. The calculations use the wavelength-dependent indexes of refraction for SF-10,[32] water,[33] and gold.[34] Figure 2 is for a 40.0-nm-thick gold film. Figure 3 is for a 45.0-nm-thick gold film. The figures plot the contours generated for 1, 5, 10, 20, 30, and 50% reflectivity, and the critical angle for the SF-10/water interface is also plotted as the solid black line. As shown in the inset of Figure 2, a theoretical SPR reflectivity versus angle curve can be generated from these contour plots by taking cuts parallel to the *x*-axis. In a similar fashion, SPR reflectivity versus wavelength curves can be obtained by taking cuts parallel to the *y*-axis and are used in a subsequent paper.[35]

(30) Hansen, W. N. *J. Opt. Soc. Am.* **1968**, *58*, 380−390.
(31) Welford, K. *Opt. Quantum Electron.* **1991**, *23*, 1−27.
(32) Kaschke, S. Schott Glasswerke, 1995.
(33) Thormählen, I.; Straub, J.; Grigull, U. *J. Phys. Chem. Ref. Data* **1985**, *14*, 933−945.
(34) Johnson, P. B.; Christy, R. W. *Phys. Rev. B* **1972**, *6*, 4370−4379.
(35) Frutos, A. G.; Weibel, S. G.; Corn, R. M. *Anal. Chem.* **1999**, *71*, 3935−3940.

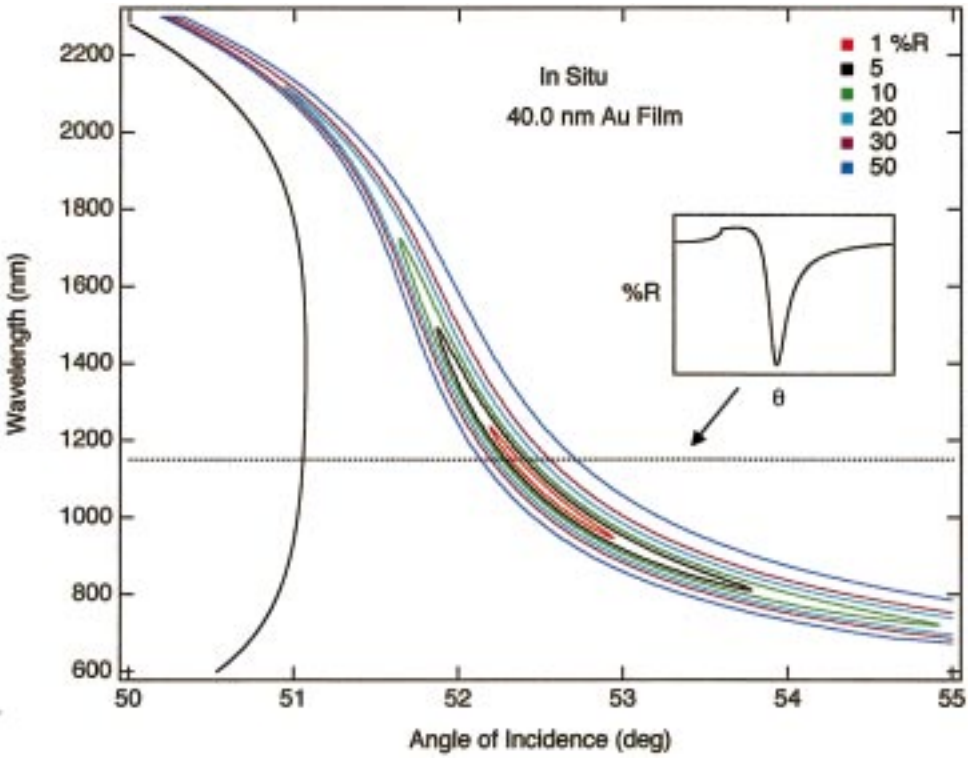


Figure 2. Reflectivity contour plot of percent reflectivities as a function of both wavelength and angle of incidence for a 40.0-nm-thick gold film. Percent reflectivities (% *R*) for several increments from 50 to 1% are shown as contour lines. The critical angle is shown as a black line. Wavelength-dependent parameters obtained from dispersion formulas generated for water, SF-10 glass, and gold were used to generate a three-phase Fresnel calculation for a 40.0-nm bare gold coating on SF-10 glass in water. This thickness is optimal for excitation from 900 to 1250 nm and was used for experiments done at 1152 nm. Inset: A reflectivity versus angle curve can be generated from the contour plot by cutting parallel to the *x*-axis (dotted line).

As seen in the figures, there exists a range of optimal wavelengths to perform the SPR angle scanning measurement for each gold thickness. For example, for a 40.0-nm gold film, a SPR reflectivity minimum of 1% or less will be observed in scanning angle measurements performed in a wavelength range of 945−1235 nm. This gold thickness was chosen for the 1152-nm experiments; Figure 1 shows a SPR reflectivity curve for this thickness. Similarly, the optimum gold film thickness for SPR scanning angle experiments in the wavelength range of 753−954 nm is 45.0 nm. This thickness was used for the SPR reflectivity curve shown in Figure 1 and in subsequent measurements at 814 nm.

A second point that can be observed in the contour plots is that the reflectivity minimum associated with the SPR angle narrows considerably at longer wavelengths, in agreement with the experimental data in Figure 1. In addition, the SPR angle moves closer to the critical angle at longer wavelengths. This crowding of the SPR angle becomes even more pronounced in ex situ (i.e., BK-7/Au/air) measurements. The "sharpest" reflectivity curves would be obtained from experiments that changed the wavelength and angle simultaneously to create a reflectivity cut through the minimum that was perpendicular to the reflectivity contour lines. For the 40.0-nm gold film, these cuts would be at a slope of 900 nm/deg, whereas for the 45.0-nm gold film, cuts would be at a 2300 nm/deg slope, much closer to vertical on the figure.

**SPR Measurements at 1152 nm.** To demonstrate the ability to monitor in situ adsorption with SPR reflectivity measurements at 1152 nm, we have measured the SPR response upon the formation of a self-assembled monolayer of 11-mercaptoundecanoic acid on a gold surface with both 1152- and 632.8-nm excitation. The thickness of this self-assembled monolayer has been characterized previously with FT-IR, ellipsometry, and ex situ SPR measurements and found to be 1.7 nm.[6,9,36] SPR reflectivity curves taken with 1152-nm excitation before and after adsorption of the MUA monolayer are shown in Figure 4. With an instrumental resolution of ±0.004°, an easily discernible shift of 0.044° is observed. In situ SPR measurements at 632.8 nm (not shown) yield an angle shift upon MUA adsorption of 0.18°.

While the magnitude of the shift in the SPR minimum is greater for in situ measurements taken at 632.8 nm, the determination of the angle shift at 1152 nm is more precise than that at 632.8 nm. This is because the SPR minimum is much sharper in the NIR; by comparison, the SPR reflectivity minimum at 632.8 nm is broad and the exact location of the minimum angle is difficult to ascertain. Specifically, in an in situ experiment at 632.8 nm, the reflectivity at the SPR angle for the bare gold surface increases by only 0.8% upon adsorption of the MUA monolayer, whereas at 1152 nm the reflectivity at the SPR angle increases by 1.7% upon adsorption of the MUA monolayer. This larger percentage change in reflectivity with adsorption is due to the sharper SPR minimums in the NIR. These experiments demonstrate that the adsorption of biopolymers and other organic molecules onto

(36) Bain, C. D.; Troughton, E. B.; Tao, Y.; Evall, J.; Whitesides, G. M.; Nuzzo, R. G. *J. Am. Chem. Soc.* **1989**, *111*, 121.

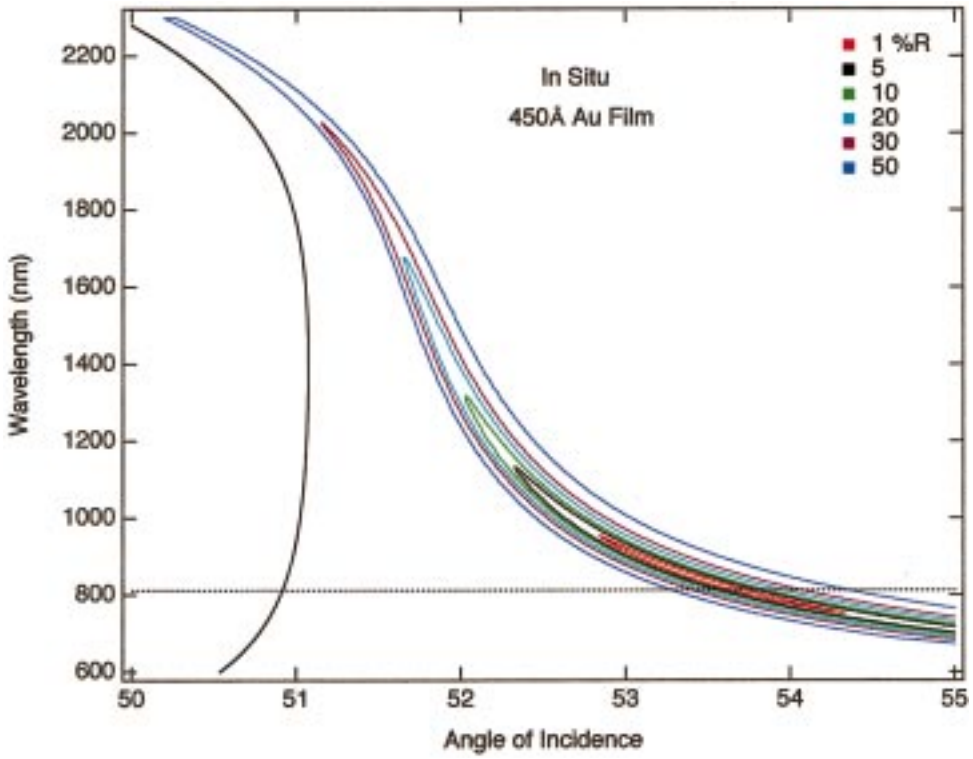


Figure 3. Reflectivity contour plot of several percent reflectivities (% *R*) as a function of both wavelength and angle of incidence (deg) for a 45.0-nm-thick gold film. This thickness is optimal for excitation from 750 to 950 nm and was used for experiments done at 814-nm excitation.

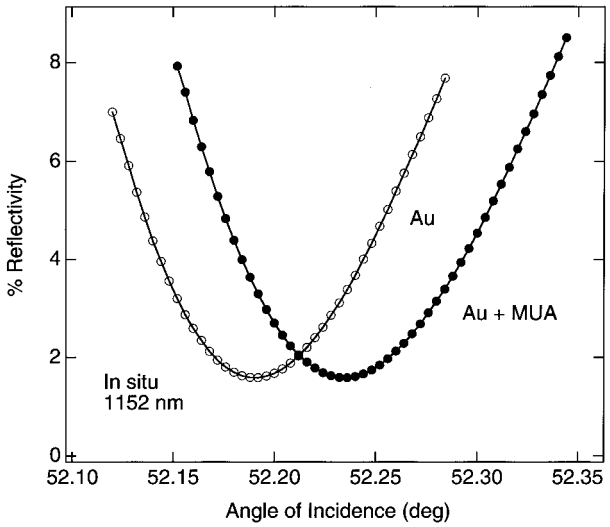


Figure 4. Expanded view of SPR reflectivity curves for the in situ angle shift measurement of MUA monolayer adsorption onto gold. Circles show data taken with 1152-nm excitation for an SF-10 glass/Au/water assembly. MUA adsorption produces a 0.044° shift, corresponding to an estimated 1.7-nm-thick film from a four-phase Fresnel calculation. Angle shifts are smaller in the NIR compared to the visible, but the increased sharpness of the SPR minimums compensates for this change. Note that the angle resolution of the instrument is 0.004°, sufficient for precise determination of monolayer film thickness.

gold surfaces can be easily followed in situ with angle shift SPR measurements at 1152 nm.

**SPR Measurements at 814 nm.** SPR measurements of multilayer films with visible excitation can be complicated by broad minimums and the need to scan at large incident angles. Since NIR excitation produces smaller angle shifts and sharper minimums, the practical dynamic range of SPR can be increased with NIR excitation. To demonstrate the dynamic range of the NIR SPR technique, we have monitored the layer-by-layer (LbL) growth of electrostatically adsorbed biopolymer/nanoparticle multilayers with an 814-nm ex situ SPR scanning angle reflectivity measurement. These films use electrostatic interactions to form tightly bound multilayers. Figure 5 plots the SPR reflectivity curves taken during the sequential deposition of an electrostatically adsorbed ultrathin multilayer. Curve a shows the SPR reflectivity minimum for a bare gold surface. This surface was first modified with a carboxylic acid-terminated MUA monolayer. The next several steps involve the sequential electrostatic adsorption of different biopolymers with alternating charge. At pH 8.8, a biopolymer with positively charged lysine residues, poly(L-lysine), was bound to the deprotonated MUA monolayer, and negatively charged poly(L-glutamate) was bound to the PL. After a second layer of positively charged PL, the reflectivity minimum shifts to curve b. From a four-phase Fresnel calculation, the thickness of this ultrathin film was estimated to be 3.05 ± 0.09 nm, using 1.45 as the index of refraction at 814 nm. The surface was then exposed to a solution of nanosized, negatively charged colloidal $SiO_2$. The colloids adsorb to the surface and add an estimated 6.38 ± 0.09 nm to the film thickness. It was assumed that the composite colloid/polymer film would have the same index of refraction as the polymer layers, since pure $SiO_2$ has an index of refraction of 1.46.[37] Further alternating adsorption of PL and $SiO_2$ particles resulted in a 20-nm mixed-composition film. SPR angle shifts and thickness changes for each layer are listed in Table 2. SPR measurements show that, with each step, the PL monolayer adsorbs onto the $SiO_2$, changing the charge on the surface and

(37) Caruso, F.; Lichtenfeld, H.; Giersig, M.; Möhwald, H. *J. Am. Chem. Soc.* **1998**, *120*, 8523−8524.

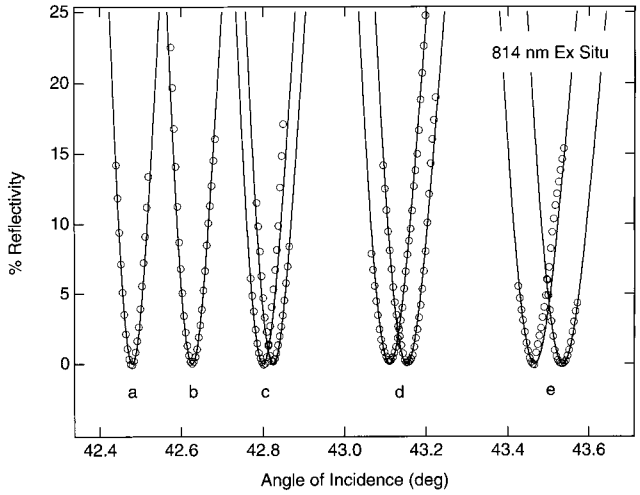


Figure 5. Expanded view of SPR reflectivity minimums taken with 814-nm excitation showing the sequential buildup of a polymer/$SiO_2$ multilayer film in air (ex situ). A 45.0-nm gold film on BK-7 glass was used. Each angle shift measurement shown represents a separate adsorption step. Multilayer formation begins with (a) bare gold surface. (b) Polymer multilayer: carboxylic acid-terminated MUA is adsorbed onto the gold and a biopolymer, poly(L-lysine), is adsorbed onto the MUA. Negatively charged poly(L-glutamate) is adsorbed onto the positively charged PL, and another layer of PL is added on top of this. (c) Negatively charged nanosized $SiO_2$ colloidal particles electrostatically adsorb to the positively charged polymer coating, and another layer of PL is added. (d) and (e) show additional sequential adsorption steps. Characterization of multilayer films can be difficult in the visible because of broadening of the SPR minimum at thickness larger than 20 nm. Excitation at 814 nm gave the best combination of dynamic range and sensitivity for the ex situ characterization of multilayer films.

Table 2. Shift Values and Thickness of Multilayer Composite Films Determined from Scanning SPR Experiments at 814 nm

| layer | shift (deg) | thickness (nm) | Figure 5 |
|---|---|---|---|
| bare gold | 0 | 0 | a |
| MUA/PL/PG/PL | 0.147 | 3.05 | b |
| $SiO_2$ | 0.322 | 6.38 | c |
| PL | 0.345 | 6.83 | c |
| $SiO_2$ | 0.630 | 11.74 | d |
| PL | 0.673 | 12.42 | d |
| $SiO_2$ | 0.986 | 17.20 | e |
| PL | 1.058 | 18.20 | e |

allowing for further deposition of colloidal $SiO_2$. Note that the SPR reflectivity curves in Figure 5 do not broaden significantly over the shift range; SPR scanning angle measurements collected at 632.8 nm have a significant amount of broadening of the SPR minimum with increasing thickness that can complicate the Fresnel calculation analysis of the shift data. Moreover, since the electromagnetic fields associated with the NIR have longer decay lengths, these thicker films can more easily be characterized in the NIR.

**NIR SPR Imaging Measurements.** In addition to the NIR SPR scanning angle measurements, we now routinely employ fixed-angle SPR imaging in the NIR to make differential adsorption measurements onto arrays of DNA and other biopolymers attached to gold surfaces. In previous SPR imaging experiments, we have employed an expanded 632.8-nm laser beam incident on

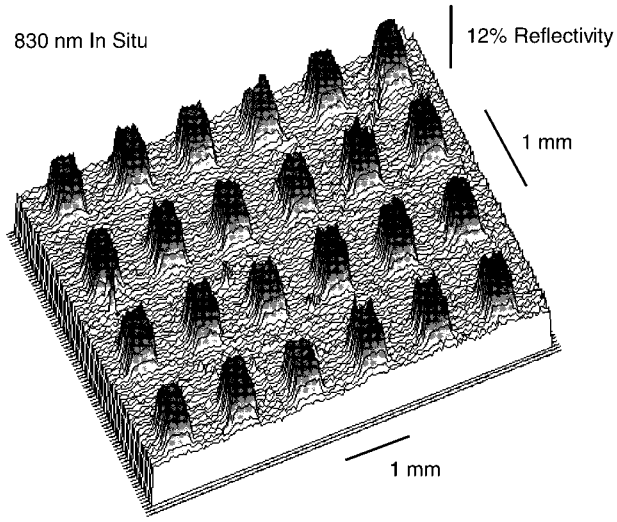


Figure 6. NIR SPR difference image of single-stranded DNA binding protein adsorbed onto a photopatterned DNA array. A single-stranded oligonucleotide was bound to the surface array elements and then exposed to a nanomolar solution of SSB. The image shown is the difference of two images taken immediately before and after exposure of the array to SSB. The image was taken at 830 nm with a 10-nm fwhm interference filter. The increased sharpness of NIR SPR enhances the contrast of the image.

the prism at a fixed angle; changes in the reflectivity upon adsorption of molecules onto various portions of the surface result in differential reflectivity images that we have used to monitor the adsorption of DNA and proteins onto surfaces.[6,9,10] In our previous experiments, the use of a coherent light source produced laser fringes that degraded the SPR image. By switching to the combination of a collimated white light source and a NIR narrow band-pass filter to obtain the SPR image, the fringes are eliminated. SPR imaging with an incoherent white light source has been demonstrated previously where changes in color due to SPPs were used to image a patterned substrate in the visible region.[24] The addition of the band-pass filter allows for easy selectivity of the imaging wavelength and allows for the use of a simple CCD camera. Sharper SPR reflectivity curves in the NIR mean better image contrast compared to that in the visible region and less manipulation to find the best angle for the SPR imaging measurement. For example, Figure 6 shows the NIR SPR difference image of single-stranded DNA binding protein adsorbed onto a photopatterned DNA array. The image was taken at 830 nm with a 10-nm band-pass filter. The array is composed of 500 × 500 $\mu$m squares of single-stranded DNA surrounded by a poly(ethylene glycol)-terminated alkanethiol that resists protein adsorption. The image shown is the difference between images taken before and after exposure of the array to SSB. The difference in reflectivity between the background and the SSB spots is approximately 10%; this image demonstrates that we have ample sensitivity with the NIR imaging apparatus to study the adsorption of proteins onto DNA monolayers.

Although the thickness sensitivity of the NIR SPR images is excellent, the increase in the surface plasmon propagation length on the surface causes a loss in the lateral resolution for microscopy purposes. Propagation lengths can approach 25 $\mu$m at 830 nm and resolution is limited to features larger than this.[14] However, NIR

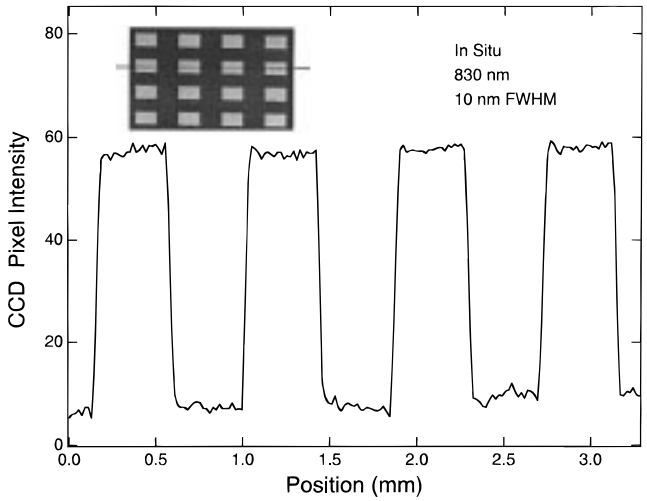


Figure 7. In situ line profile of a photopatterned MUA/PL/PG/PL/$SiO_2$ multilayer film taken with a 10-nm fwhm interference filter at 830 nm. The increased throughput of a wider band-pass filter improves the image signal-to-noise ratio. Use of an incoherent white light source eliminates laser fringes in the image (inset). The pattern was created by removing portions of a MUA-coated gold film by photooxidation. Photooxidized portions were replaced with a MUD monolayer, which resists PL, PG, and $SiO_2$ adsorption. The ultrathin multilayer film was built up by electrostatically adsorbing monolayer films of alternating charge in situ.

SPR images of test patterns (not shown) demonstrate that 50-$\mu$m features can be easily resolved with 830-nm excitation.

A final advantage of the NIR white light/interference filter configuration is that a range of wavelengths can be used to increase light throughput and improve the signal-to-noise ratio in the SPR image. This is possible because the SPR images are not limited to strictly monochromatic light. To demonstrate this, a composite LbL film was assembled in situ onto a photopatterned surface. The 500 $\times$ 500 $\mu$m squares of positively charged MUA are surrounded by 11-mercaptoundecanol, a hydroxyl-terminated alkanethiol that resists the electrostatic adsorption of PL, PG, and $SiO_2$. After the in situ assembly of a five-component composite multilayer, a SPR image of the patterned surface was taken. Since the amount of light collected by the CCD camera limits the signal-to-noise ratio, use of a higher throughput filter can improve contrast in the image. This can be achieved by use of a wider band-pass filter. Figure 7 shows a line profile of the multilayer stack taken with a 10-nm fwhm band-pass filter at 830 nm. When compared to images taken with a 1-nm band-pass filter at the same wavelength, no loss in image contrast was observed using the wide band-pass filter. In fact, the wider band-pass resulted in a significant improvement in the contrast and a 3-fold increase in the signal-to-noise ratio versus a 1-nm band-pass. This improvement is attributed to increased light throughput for the wider band-pass filter. The inset shows the image from which the line profile was taken. Note that the use of an incoherent white light source clarifies the SPR image by eliminating laser fringes often seen in images created from laser excitation.

## SUMMARY AND CONCLUSIONS

In this paper, we have demonstrated the utility of NIR wavelengths for SPR scanning angle and imaging measurements. The advantage of NIR SPR for use in the characterization of multilayer films and for SPR imaging is demonstrated. For SPR scanning angle measurements, the ability of the SPR angle shift measurement to detect the adsorption of ultrathin biopolymer films is equivalent in the NIR to that in the visible region. This result is surprising given the substantial increase in wavelength and is attributed to the significant changes in the gold indexes of refraction in the NIR. Characterization of thicker films is facilitated in the NIR because of the longer decay length of the electromagnetic fields associated with the surface plasmons moving away from the surface. One area where NIR SPR measurements can become useful is when there is a strong absorption in the monolayer film at visible wavelengths. For example, wavelengths longer than 1100 nm can be used in principle to probe the silicon/metal interface.[17] NIR wavelengths can also be used in multiple-wavelength experiments to help quantify the film thickness more accurately. For SPR imaging experiments, the combination of NIR illumination with an incoherent source and a band-pass interference filter leads to almost 1 order of magnitude enhancement in the SPR differential reflectivity image. One caveat is that features with dimensions less than approximately 25 $\mu$m will not be observable due to the increased SPR propagation length in the NIR. As a final note, the NIR can also be used for wavelength shift measurements. This subject is explored in a subsequent paper[35] that used a Fourier transform spectrometer to extend the NIR SPR measurements down to 2 $\mu$m or 5000 $cm^{-1}$.

## ACKNOWLEDGMENT

The authors gratefully acknowledge the support of the National Science Foundation in these studies.

Received for review May 13, 1999. Accepted July 9, 1999.

AC990517X